Ann. Geophys., 33, 471–479, 2015
www.ann-geophys.net/33/471/2015/
doi:10.5194/angeo-33-471-2015
© Author(s) 2015. CC Attribution 3.0 License.

Annales Geophysicae
Open Access

Analysis of the enhanced negative correlation between electron density and electron temperature related to earthquakes

X. H. Shen, X. Zhang, J. Liu, S. F. Zhao, and G. P. Yuan

Institute of Earthquake Science, China Earthquake Administration, 100036 Beijing, China

Correspondence to: X. Zhang (zhangxm96@hotmail.com)

Received: 15 September 2014 – Revised: 12 February 2015 – Accepted: 16 March 2015 – Published: 20 April 2015

Abstract. Ionospheric perturbations in plasma parameters have been observed before large earthquakes, but the correlation between different parameters has been less studied in previous research. The present study is focused on the relationship between electron density (N_e) and temperature (T_e) observed by the DEMETER (Detection of Electro-Magnetic Emissions Transmitted from Earthquake Regions) satellite during local nighttime, in which a positive correlation has been revealed near the equator and a weak correlation at mid- and low latitudes over both hemispheres. Based on this normal background analysis, the negative correlation with the lowest percent in all N_e and T_e points is studied before and after large earthquakes at mid- and low latitudes. The multiparameter observations exhibited typical synchronous disturbances before the Chile M8.8 earthquake in 2010 and the Pu'er M6.4 in 2007, and T_e varied inversely with N_e over the epicentral areas. Moreover, statistical analysis has been done by selecting the orbits at a distance of 1000 km and ±7 days before and after the global earthquakes. Enhanced negative correlation coefficients lower than −0.5 between N_e and T_e are found in 42 % of points to be connected with earthquakes. The correlation median values at different seismic levels show a clear decrease with earthquakes larger than 7. Finally, the electric-field-coupling model is discussed; furthermore, a digital simulation has been carried out by SAMI2 (Sami2 is Another Model of the Ionosphere), which illustrates that the external electric field in the ionosphere can strengthen the negative correlation in N_e and T_e at a lower latitude relative to the disturbed source due to the effects of the geomagnetic field. Although seismic activity is not the only source to cause the inverse N_e–T_e variations, the present results demonstrate one possibly useful tool in seismo-electromagnetic anomaly differentiation, and a comprehensive analysis with multiple parameters helps to further understand the seismo–ionospheric coupling mechanism.

Keywords. Ionosphere (plasma temperature and density)

1 Introduction

The DEMETER (Detection of Electro-Magnetic Emissions Transmitted from Earthquake Regions) satellite was launched on 29 June 2004 in France and operated until 10 December 2010, with an inclination of 98° (Cussac et al., 2006). It was a solar-synchronous-orbit satellite, with the local time of each orbit passing the equator being the same: 10:30 in the daytime and 22:30 in the nighttime. From its records, many ionospheric perturbations related to seismic cases have been detected (Parrot et al., 2006; Sarkar et al., 2007, 2012; Zhang et al., 2009, 2010a, b, 2012a; Zeng et al., 2009; Pisa et al., 2011; Liu et al., 2011). Furthermore, statistical analysis of different parameters has been developed to ascertain the relationship between ionospheric perturbations and large earthquakes (Némec et al., 2009; He et al., 2010, 2011; Zhang et al., 2011, 2012b; Parrot, 2012; Pisa et al., 2012; Li and Parrot, 2012). Based on a great amount of data, statistical research can help us to understand the general distribution features of ionospheric perturbations in time and space and to provide more information on their occurrence probability related to earthquakes.

Many papers have shown the correlation characteristics at different local times and conditions of the in situ electron density and temperature (N_e and T_e) observed by the satellite (Balan et al., 1997; Oyama et al., 1996; Su et al., 1996; Rich et al., 2003; Lin et al., 2007a, b; Liu et al., 2007; Ren et al., 2008; Venkatraman and Heelis 1999; Li et al., 2011; Kakinami et al., 2011a, b). The negative correlation between

Published by Copernicus Publications on behalf of the European Geosciences Union.

N_e or N_i (ion density) and T_e during local daytime is widely accepted. Some positive correlations have been found during periods of high solar activity (Kakinami et al., 2011a) and also in the equatorial area at sunset in December (Liu et al., 2007). In earthquake research, N_e and N_i are frequently used in case and statistical studies. Only a few papers have focused on T_e and ion temperature (T_i). For example, Oyama et al. (2008) studied the variations in T_e observed by the Hinotori satellite before and after three earthquakes during 1981–1982 and found that T_e significantly decreased over the epicenters in the afternoon in the 5 days before and after the earthquakes. Sharma et al. (2013) summarized T_i and T_e variations related to seismic activity during 1995–1998 over India by using SROSS (Stretched Rohini Satellite Series)-C2 satellite data in the altitude range of 430–630 km, in which significant enhancement had been detected, with 1.2–1.5 times the average normal values of T_e and 1.1–1.3 times the normal T_i within a 5° window over the epicenters. Sarkar et al. (2012) studied the ionospheric anomalies related to the Haiti earthquake on 12 January 2010, and their results from the DEMETER satellite showed the most important variations in N_e and T_e 1 day before the main shock, with T_e exceeding the upper bound of ~ 100 K and N_e exceeding the upper bound by 20 and 9 % during the day- and nighttime, respectively. By using DEMETER satellite data, Zeng et al. (2009) found that N_e and T_e decreased to a value above 20 % during local daytime near the epicenter in the 4 and 5 days prior to the Wenchuan M7.9 earthquake on 12 May 2008 in China.

The big problem in earthquake prediction is the variety of anomalies before and after different earthquakes; a single kind of precursor is hard to detect in all events. Also, ionospheric perturbations cannot be detected for all earthquakes. Thus, the sensitivity estimation of precursors is also an important topic in seismological studies. Here, based on the study of the correlation between N_e and T_e recorded by the Langmuir probe onboard the DEMETER satellite, some short time disturbances with inverse N_e and T_e are recorded for the more than 6 years of the DEMETER satellite's operating time. Statistical analysis related to large earthquakes is also carried out. Finally, discussion and conclusions are provided in the last section of the paper.

2 Correlation characteristics of N_e and T_e during local nighttime

2.1 The ISL onboard the DEMETER satellite

The specific scientific objectives of the Langmuir probe instrument (ISL: Instrument Sonde de Langmuir) are designed to map the bulk plasma parameters (primarily N_e and T_e) and to study their variations associated with solid-earth events and other sources of perturbations (Lebreton et al., 2006). The Langmuir probe sweeps at a voltage of ± 3.81 V. A complete voltage sweep is performed in 1 s to obtain a complete current–voltage (I–V) characteristic, corresponding to about a 7 km spatial resolution at 710–660 km altitude from the sun-synchronous DEMETER orbit. From the analysis of the I–V characteristics, the plasma parameters are extracted with 1 s time resolution; these are N_e, T_e, N_i and spacecraft potential.

3 Correlation background between N_e and T_e

Due to the strong effects of solar activity during local daytime, local nighttime data is generally employed in earthquake research to avoid solar and space disturbances. Therefore, here only the correlation between N_e and T_e during local nighttime is analyzed. Figure 1 shows the projection of N_e (x axis) and T_e (y axis) at the different geomagnetic latitudes (color scale) in March, June, September and December 2008 (four images labeled 2008-03, 2008-06, 2008-09 and 2008-12). It can be seen that there is seasonal variation in N_e and T_e, with the images from March and September being the same and those from June and December being very similar to each other. Generally, all four seasons' pictures show that at low latitudes N_e changes a lot but T_e varies little, while at midlatitudes N_e and T_e are dispersed, especially in June and December. In a previous study, the absolute values of N_e and T_e from DEMETER were not very accurate, with T_e being much higher than it is supposed to be (Kakinami et al., 2013); therefore, in this paper only the relative variations in N_e and T_e are taken into account. To reveal the relationship of N_e and T_e at different latitudes, Fig. 2 provides the correlation coefficients for March 2008 from a linear function fitting with the equation

$$R = \frac{\sum_{i=1}^{n}((N_e)_i - \bar{N}_e)((T_e)_i - \bar{T}_e)}{\sqrt{\sum_{i=1}^{n}((N_e)_i - \bar{N}_e)^2 \sum_{i=1}^{n}((T_e)_i - \bar{T}_e)^2}},$$

with the six diagrams separated by a latitude interval of 5° in the Northern and Southern Hemisphere (Fig. 2a and b). The results show the weak connection between N_e and T_e during local nighttime, with a maximum R of only about 0.4 in the equatorial area of latitudes 5° S–5° N. With the increase in latitude, R decreased quickly, but it still maintained a positive correlation over both hemispheres. Compared with Hinotori satellite data, after 20:00 LT, both N_e and T_e followed the usual nighttime decay and a positive correlation was detected (Kakanami et al., 2011b), which was also observed using the incoherent scatter radar at Saint-Santin (Zhang et al., 2004). Therefore, the weak positive correlation between N_e and T_e is the normal state in the nighttime topside ionosphere.

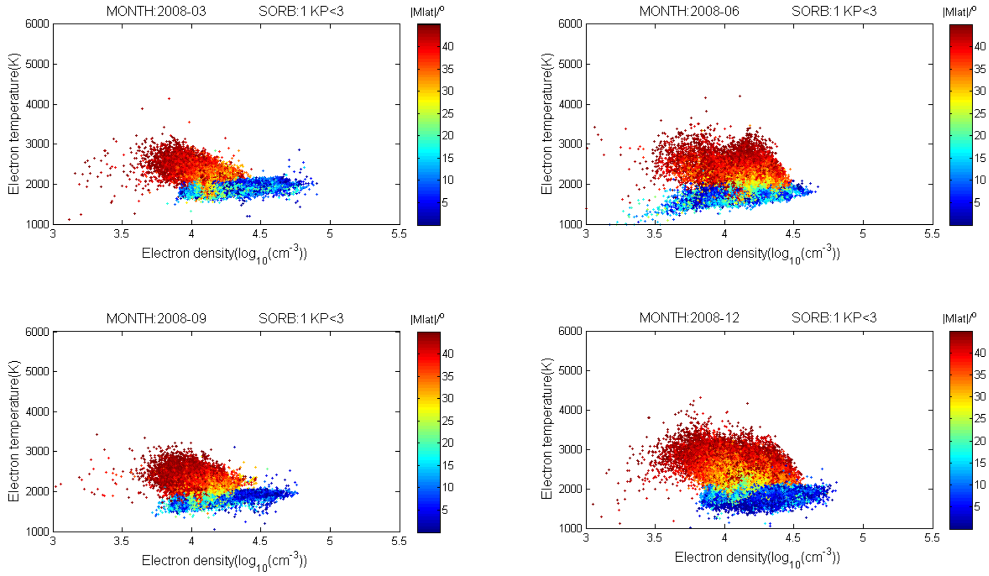

Figure 1. The distribution of log10(N_e) and T_e at different magnetic latitudes (color bar) during quiet geomagnetic periods with Kp <3 during 4 months (four panels correspond to March, June, September and December) in 2008.

4 Examples of ionospheric perturbations and statistical analysis

4.1 Disturbances in plasma parameters related to earthquakes

Figures 3 and 4 present the plasma variations before the significant earthquake on 27 February 2010 in Chile with a magnitude of 8.8 (72.72° W, 35.85° S). Figure 3 corresponds to orbit 30 168, recorded on 20 February 2010 (7 days before the earthquake), and Fig. 4 show orbit 30 256 on 26 February 2010 (1 day before the earthquake) at a distance of 2000 km from the epicenter. Both figures provide the same parameters in the following order (from top to bottom): N_e; T_e; N_i(O+), detected by the IAP (Instrument d'Analyse du Plasma) on DEMETER with H+ and He+ excluded due to their small values; Ex in the ULF (ultra-low frequency) electric field, detected by ICE (Instrument Champ Electrique); and earthquakes within 2000 km of the satellite orbit during ±30 days of the orbite time. It can be seen that, along orbit 30 168_1, N_e and N_i(O+) diverged from their normally flat variational trends and decreased over the seismic region of Chile (the disturbances are framed by the blue rectangle), whereas T_e increased in the same region (Fig. 3). Along orbit 30 256_1, N_e and N_i(O+) modulated over this seismic region and T_e also showed an inverse pattern (Fig. 4). Another anomalous phenomenon in Fig. 4 is that, at the northern conjugate epicenters of the Chile earthquakes, a step-increasing variation was detected in N_e and N_i(O+), while T_e decreased. This kind of variation was also observed before some moderate earthquakes. Figure 5 gives an example along orbit 15 572_1, observed to the north of the epicenter a few hours before the Pu'er M6.4 earthquake in China on 2 June 2007 (23.03° N, 101.05° E), in which a reversed step variation is illustrated between T_e and N_e, while N_i(O+) shows variations of a similar shape as N_e. All of these observations demonstrate that some coupling processes during the preparation processes of earthquakes lead to the simultaneous variations in N_e and T_e. In order to test the sensibility of this kind of anomaly, a statistical analysis needs to be done based on large amounts of data from the DEMETER satellite and many seismic events.

5 Method and statistical analysis

In order to reflect this reversed variation feature between N_e and T_e during local nighttime before earthquakes, the floating coefficients are calculated for 20 observation points along orbits 15 572_1 and 30 168_1 (Fig. 6). The results show that the normal coefficients are above 0 during local nighttime, which means that the positive correlation between N_e and T_e is limited in time and space. Along 15 572_1, the maximal coefficients were near 1.0; however, a quick decrease was exhibited, with R lower than −0.9, around a latitude of 30° N (Fig. 6a), which was just to the north of the Pu'er epicenter. By contrast, along orbits 30 168_1 and 30 256_1, the coefficients varied significantly, with a few points lower than −0.5 (Fig. 6b and c), in the southern part of the orbits at 10–50° S; this illustrates the extensive modulation due to the combined effect of the major earthquake and following aftershocks along the whole Chile seismic rupture fault.

On the basis of the negative N_e–T_e correlation related to earthquakes shown above, a statistical analysis is carried out. First, an automatic software is developed to calculate the R

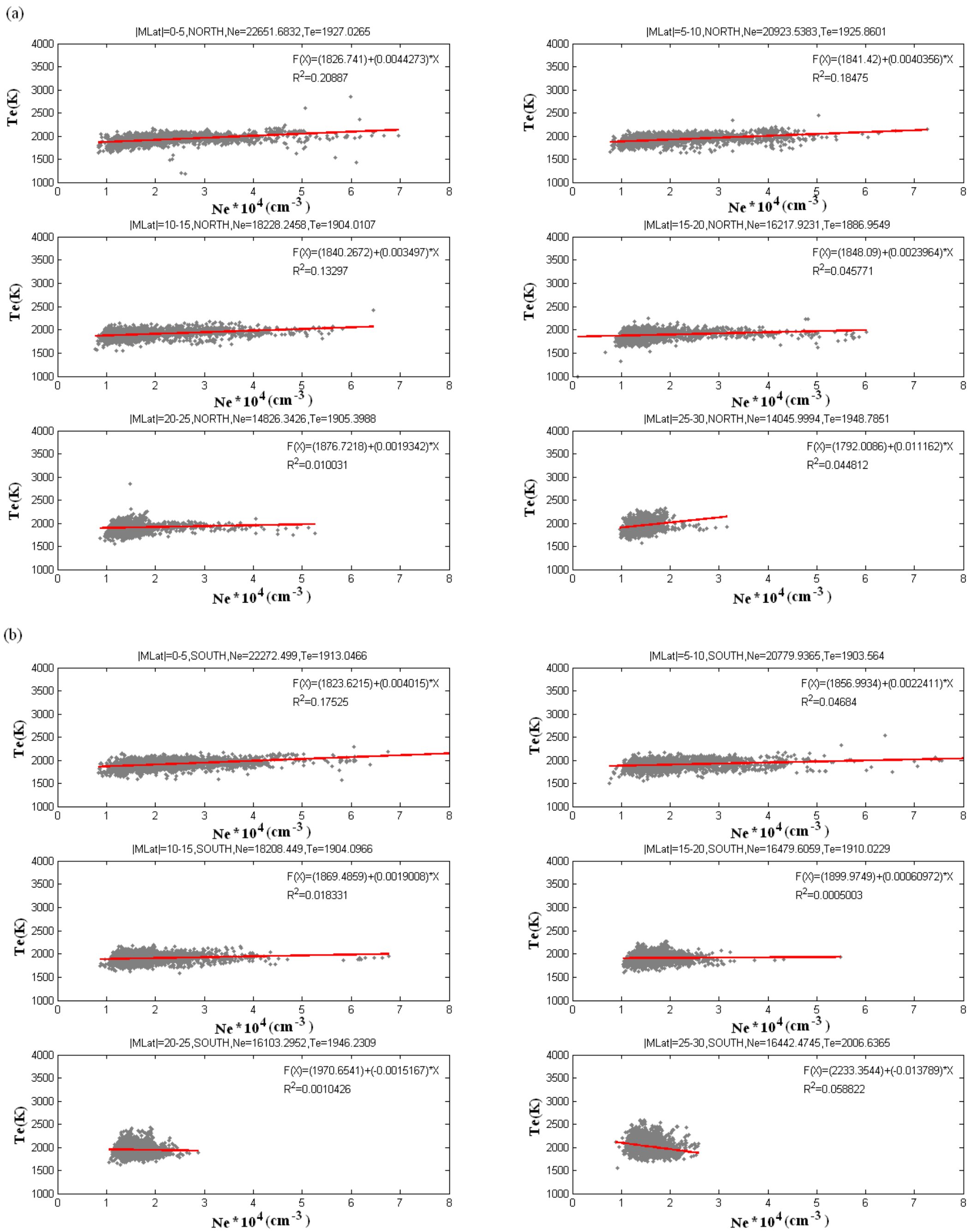

Figure 2. The linear correlation between N_e and T_e at 0–30° at 5° latitude intervals over the Southern **(a)** and Northern **(b)** Hemisphere (at the top of each panel, MLat represents the magnetic latitude scale, NORTH/SOUTH means Northern or Southern Hemisphere, and N_e and T_e are the averaged values of all the points distributed in that latitude range; the equation in each panel represents the fitted results, in which x represents N_e, $f(x)$ is T_e and R is the linear correlation coefficient of N_e and T_e).

of N_e and T_e with 12–13 observation points at 1° of latitude during January 2005 to December 2010. Taking account of the distribution of global main quakes and the effects from polar electrojets at high latitudes, the studied area is limited to ±45° of latitude. Figure 7 shows the number of points corresponding to different R values. It can be seen that most points have an R higher than 0.5, which means that N_e and T_e vary positively within a 1° latitudinal scale. The counts coincide with an exponential attenuation, with the decrease of R to the minimum number corresponding to the maximum negative correlation of -1.0 and the exponential fitting of R being larger than 0.98. The points with R less than -0.5 only occupy 0.5 % of all points, which illustrates that good negative correlations in N_e and T_e are rare events. While strong

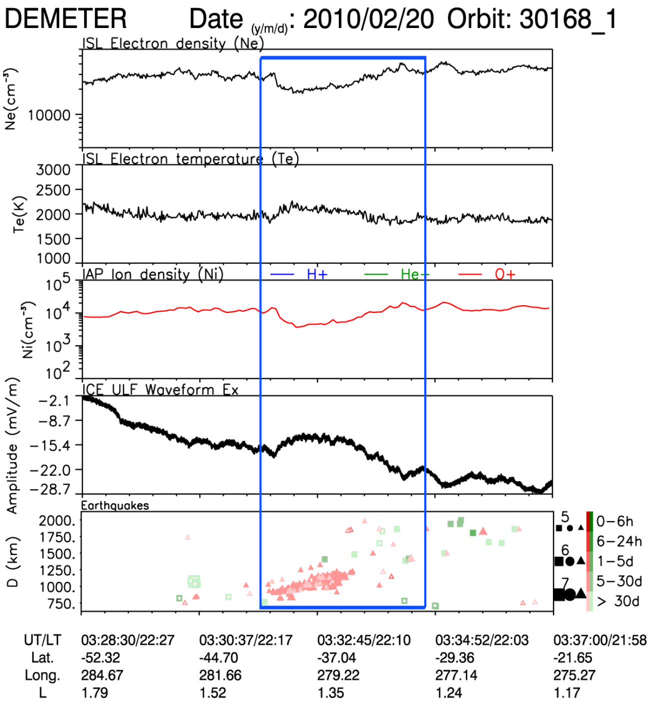

Figure 3. The observation of plasma parameters from DEMETER along orbit 30 168 on 20 February 2010 before the Chile M8.8 earthquake on 27 February 2010 (first panel: N_e; second panel: T_e; third panel: the ion density of O+; fourth panel: the electric field Ex; bottom panel: the earthquakes taking place within ±30 days relative to the time of this orbit at a distance of 2000 km from the orbit; green squares represent past earthquakes, red triangles mean future earthquakes and open squares are the epicenters at geomagnetic conjugate position).

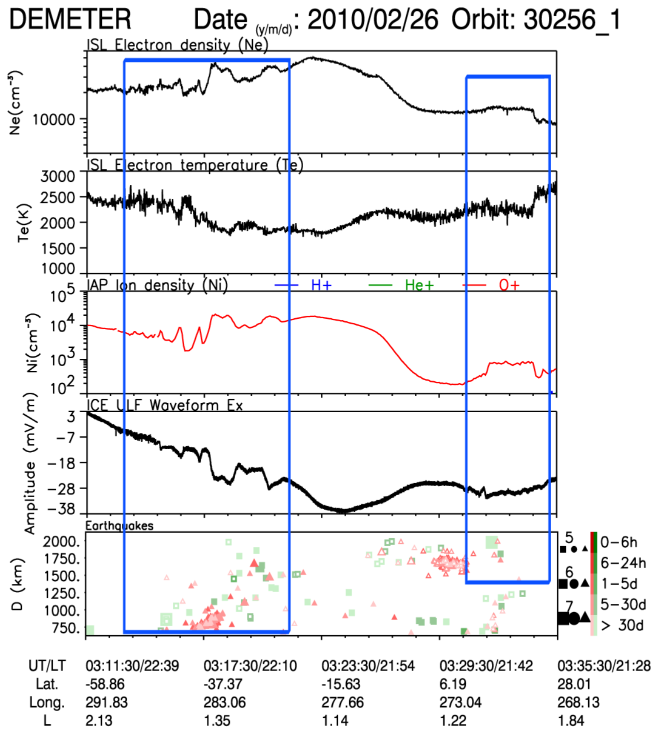

Figure 4. The observation of plasma parameters from DEMETER on 26 February 2010, 1 day before the Chile M8.8 earthquake on 27 February 2010 (the order of the five panels is the same as in Fig. 3).

earthquakes are sudden events with a small probability, earthquake preparation may be a factor that induces this inverse relationship between N_e and T_e.

Having selected earthquakes with a magnitude greater than 5.0, we select those points for which the R of N_e–T_e is less than 5.0. These points are at a distance of 1000 km to the epicenters and were observed within 7 days before and after the earthquake occurrences, suggesting that they are related to the earthquakes. The results show that of the total of 2 357 126 observation points, there are 13 101 points with strong negative correlations between N_e and T_e. In order to reduce the effects of solar activity, the data when $Kp > 3+$ is eliminated, so 6058 points are left in the end. Of these points, 2556 can be connected with earthquakes; this constitutes 42 % of global observation points with $R \leq -0.5$ in N_e–T_e. It should be noted that earthquake is only one kind of factor that leads to a negative correlation between N_e and T_e, and there still exist many others in space or ground VLF (very low frequency) transmitters that may produce similar variations. Another problem is that not all earthquakes can excite the same phenomenon in the ionosphere. In the areas studied, there were 8513 earthquakes with $M \geq 5.0$ during 2005–2010, while 7659 earthquakes were in the $5.0 \leq M < 6.0$ range, 611 in the $6.0 \leq M < 6.5$ range, 168 in the $6.5 \leq M < 7.0$ range and 75 had $M \geq 7.0$, as listed in Table 1. In order to illustrate the relationship of N_e and T_e with earthquakes, the median and averaged R values are calculated for all the data together, and Table 1 exhibits a median of 0.812 and an average of 0.694. Then the median and average R of the points within 3 days of earthquakes and at a distance of 1000 km from the epicenter of the quakes are computed at different magnitude levels to reduce the normal background effects. As shown in Table 1, the averaged R values are similar to each other at four magnitude levels and are also near the average of all global data taken together. However, the median R values decrease compared to the first median R of all points, reducing to 0.683 at magnitudes greater than 7.0. This phenomenon reveals that there might exist much lower and even negatively correlated N_e–T_e points before and after these destructive earthquakes during quite a short time period, causing the decrease in the median R.

Table 1. The statistical results of R with all observation points and of those related to earthquakes at different magnitude levels.

Statistic	All points	Points related to earthquake $5.0 \leq M < 6.0$	Points related to earthquake $6.0 \leq M < 6.5$	Points related to earthquake $6.5 \leq M < 7.0.$	Points related to earthquake $M \geq 7.0$
Median R	0.812	0.703	0.707	0.714	0.683
Average R	0.694	0.694	0.691	0.694	0.691
No. of earthquakes		7659	611	168	75

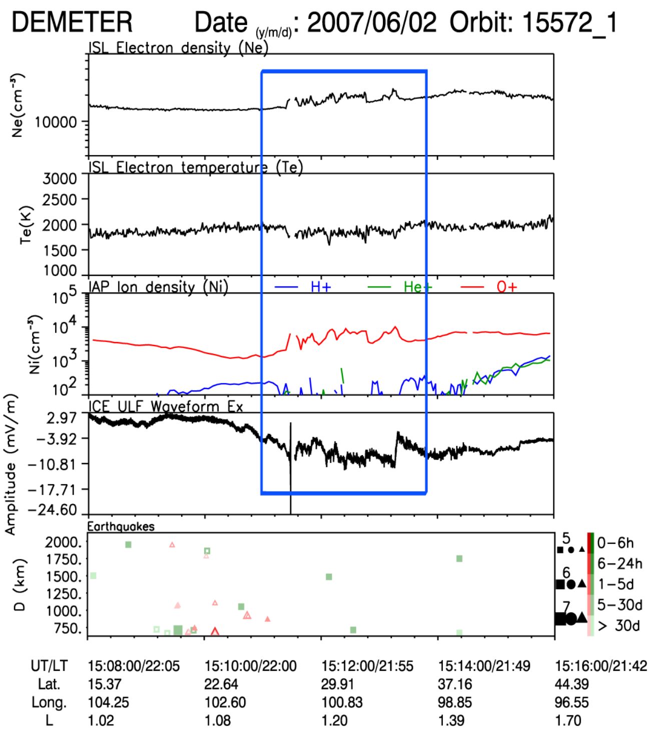

Figure 5. The observation of plasma parameters from DEMETER along orbit 15 572 on 2 June before the Pu'er M6.3 earthquake in China on 3 June 2007 (the order of the five panels is the same as in Fig. 3).

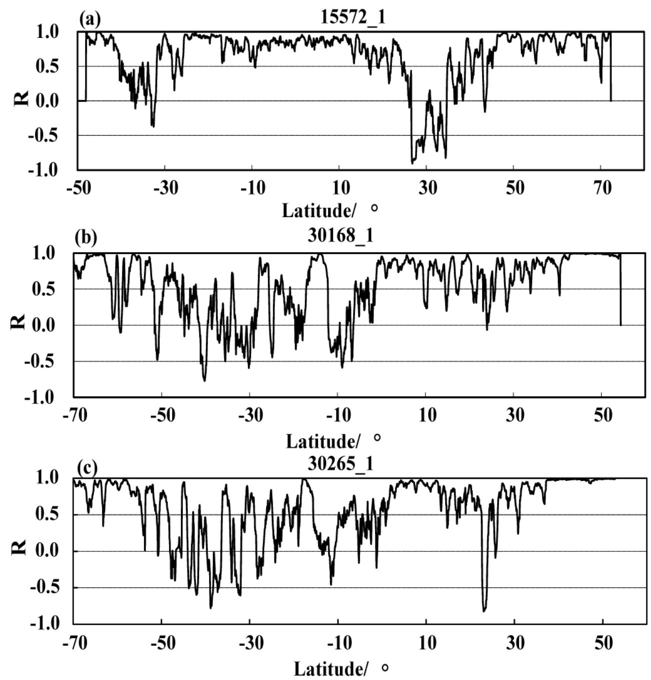

Figure 6. The correlation coefficients of N_e and T_e along the three orbits (**a**: 15 572_1; **b**: 30 168_1; **c**: 30 256_1).

6 Discussion and conclusion

From the observations of ionospheric perturbations associated with large earthquakes, several models have been proposed to explain the seismo–ionospheric coupling mechanism; these include an electromagnetic-wave-penetrating model from the lithosphere to the ionosphere (Molchanov et al., 1995), an acoustic-wave-propagating model (Hegai et al., 1997) and electrical-field-coupling models related to radon emission, aerosol accumulation, rock current and surface charge (Pulinets, 2004, 2009; Sorokin et al., 2007; Kuo et al., 2011). The last model plays an important role in explaining the ionospheric disturbances related to seismic activities in plasma parameters, such as the perturbations in GPS TEC (total electron content), foF2 and electron density;

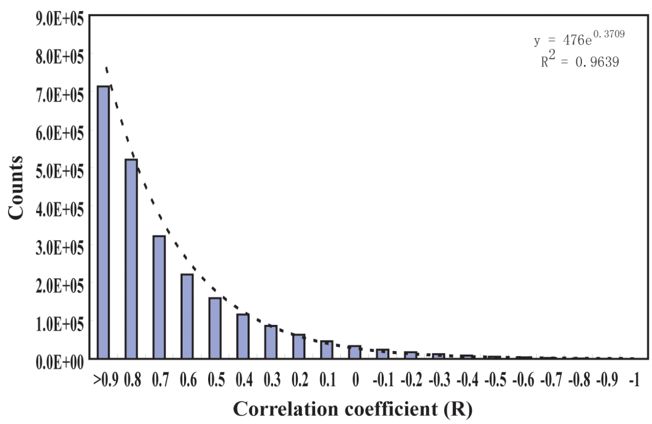

Figure 7. The histogram of distribution probability at different correlation coefficients before and after global earthquakes (in the right corner of the panel, the exponential decay has been fitted between the counts (variable y) and different coefficient scales (variable x); furthermore, the correlation coefficient R has been calculated).

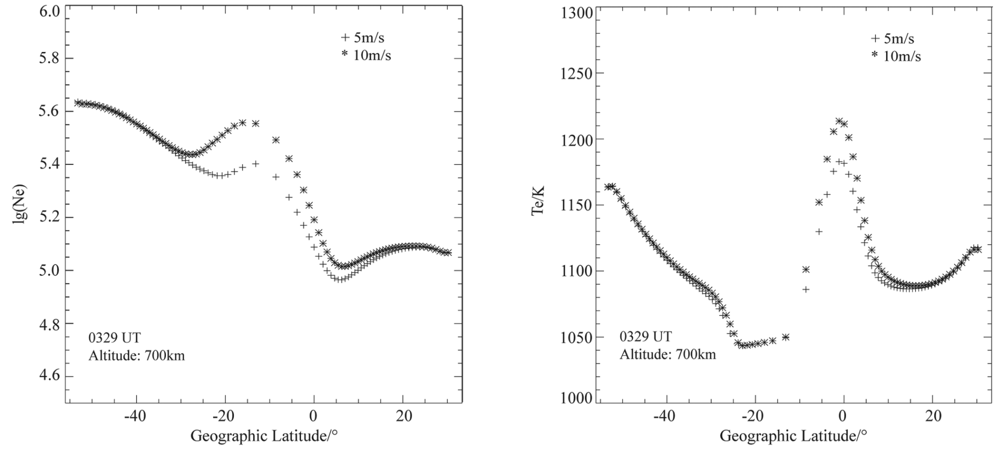

Figure 8. The calculation results from SAMI2 of N_e (left) and T_e (right) at an altitude of 700 km during local nighttime at $E \times B$ effects of $5\,\mathrm{m\,s^{-1}}$ (+) and $10\,\mathrm{m\,s^{-1}}$ (*), respectively.

the drift effects from overlapped $E \times B$ at the epicentral region coincide with the spatial distribution of perturbations in the ionosphere as shown in GPS TEC (Kuo et al., 2011).

By observing the electric field and the plasma parameters simultaneously with the DEMETER satellite, the Ex-component waveforms of the ULF electric field (DC-15Hz) are analyzed along the orbits as shown in Figs. 3–5. Combined with the ULF electric field analysis before and after earthquakes in a previous study (Zhang et al., 2014), synchronous 3–1 $5\mathrm{mV\,m^{-1}}$ disturbances were always detected in the electric field, which illustrates the existence of an external electric field in the topside ionosphere. To demonstrate the enhanced negative correlation associated with earthquakes, SAMI2 (Sami2 is Another Model of the Ionosphere) (Huba et al., 2000) is employed to simulate the effects of overlapped external electric fields in a seismic region. Here, the Chile earthquake region (36° S, 287° E) is taken as an example, and the sinusoidal $E \times B$ drift model is used to calculate the $E \times B$ effects as $5\,\mathrm{m\,s^{-1}}$ and $10\,\mathrm{m\,s^{-1}}$, respectively. The computed results are shown in Fig. 8. With the increase of $E \times B$ effects, the electron density shows a typical maximum around 10° S and two minima at 30° S and 5° N at an altitude of 700 km at 03:29 UT (in Figs. 3 and 4, this time is 22:10 LT in Chile), while the maximum of T_e occurs at the equator and two minima occur at 10–25° S and 10–20° N, respectively. Comparing the two parameters, N_e increases at 30–20° S, while T_e still decreases and maintains a low level. At 10–0° S N_e decreases, while T_e increases quickly, and at 5–10° N N_e increases, while T_e decreases quickly. It illustrates that the overlapped $E \times B$ effect from the Chile seismic region ($\sim -36°$ S) will strengthen the negative correlation feature between N_e and T_e over some specific latitudes, such as at the north of the source region and even around the equator. It should be noted here that the assumption in SAMI2 of infinite parallel conductivity may lead to nearly the same feature over both hemispheres and a smaller modified area than expected. Therefore, the disturbed region in Fig. 8 might actually be larger.

In this paper, the correlation of N_e and T_e is studied during local nighttime on the basis of the ISL observations from the DEMETER satellite. By taking account of the normal background with positive and weak correlations between N_e and T_e at different latitudes, the relationship of the negative correlation between N_e and T_e with strong earthquakes is analyzed and discussed. The following can be concluded:

1. During local nighttime, log10(N_e) and T_e show a positive linear correlation, especially at low latitudes over the Northern Hemisphere. At midlatitudes, N_e exhibits almost no correlation with T_e.

2. Synchronous perturbations in plasma parameters such as N_e, T_e, N_i(O+) and the electric field have been detected before a few strong earthquakes. Over the seismic regions, a negative correlation between N_e and T_e is exhibited at mid- and low latitudes, which is significantly different from their normal background.

3. The statistical analysis of global strong earthquakes and negative N_e–T_e correlations shows that the median R of N_e–T_e correlations only reduces with earthquakes of a magnitude greater than 7.0, illustrating the enhancement of a negative correlation between N_e and T_e during large earthquakes.

4. According to results calculated by SAMI2, the overlapped $E \times B$ effects will enhance the negative correlation between N_e and T_e, which proves that an earthquake is one possible source that can cause reversed variations in N_e and T_e in the topside ionosphere.

Acknowledgements. This study was supported by the International Science & Technology Cooperation Program (2012DFR20440K04; 2014DFR21280) and the National High-tech R&D Program (863 Program: 2012AA121004). The authors thank the DEMETER satellite center for providing the observational data.

Topical Editor H. Kil thanks K. O. Oyama and one anonymous referee for their help in evaluating this paper.

References

Balan, N., Oyama, K. I., Bailey, G. J., Fukao, S., Watanabe, S., and Abdu, M. A.: A plasma temperature anomaly in the equatorial topside ionosphere, J. Geophys. Res., 102, 7485–7492, 1997.

Cussac, T., Clair, M. A., Ultre-Guerard, P., Buisson, F., Lassalle-Balier, G., Christina Elisabelar, M. L., Passot, X., and Rey, N.: The DEMETER microsatellite and ground segment, Planet. Space Sci., 54, 413–427, 2006.

He, Y., Yang, D., Qian, J., and Parrot, M.: Response of the ionospheric electron density to different types of seismic events, Nat. Hazards Earth Syst. Sci., 11, 2173–2180, doi:10.5194/nhess-11-2173-2011, 2011.

He, Y., Yang, D., Zhu, R., Qian, J., and Parrot M.: Variations of electron density and temperature in ionosphere based on the DEMETER ISL data, Earthq. Sci., 23, 349–355, 2010.

Hegai, V. V., Kim, V. P., and Nikiforova, L. I.: A possible generation mechanism of acoustic-gravity waves in the ionosphere before strong earthquakes, J. Earthq. Predict. Res., 6, 584–589, 1997.

Huba, J. D., Joyce, G., and Fedder, J. A.: Sami2 is Another Model of the Ionosphere (SAMI2), A new low-latitude ionosphere model, J. Geophys. Res., 105, 23035–23053, doi:10.1029/2000JA000035, 2000.

Kakinami, Y., Lin, C. H., Liu, J. Y., Kamogawa, M., Watanabe, S., and Parrot, M.: Daytime longitudinal structures of electron density and temperature in the topside ionosphere observed by the Hinotori and DEMETER satellites, J. Geophys. Res., 116, A05316, doi:10.1029/2010JA015632, 2011a.

Kakinami, Y., Watanabe, S., Liu, J. Y., and Balan, N.: Correlation between electron density and temperature in the topside ionosphere, J. Geophys. Res., 116, A12331, doi:10.1029/2011JA016905, 2011b.

Kakinami, Y., Kamogawa, M., Onishi, T., Mochizuki, K., Lebreton, J.-P., Watanabe, S., Yamamoto, M.-Y., and Mogi, T.: Validation of electron density and temperature observed by DEMETER, Adv. Space Res., 52, 1267–1273, 2013.

Kuo, C. L., Huba, J. D., Joyce, G., and Lee, L. C.: Ionosphere plasma bubbles and density variations induced by pre-earthquake rock currents and associated surface charges, J. Geophys. Res., 116, A10317, doi:10.1029/2011JA016628, 2011.

Lebreton, J. P., Stverak, S., Travnicek, P., Mksimovic, M., Klinge, D., Merikallio, S., Lagoutte, D., Poirier, B., Blelly, P. L., Kozacek, Z., and Salaquarda, M.: The ISL langmuir Probe experiment and its data procession onboard DEMETER:scientific objectives, description and first results, Planet. Space Sci., 54, 472–486, 2006.

Li, L. Y., Yang, J. Y., Cao, J. B., Lu, L., Wu, Y., and Yang, D.: Statistical backgrounds of topside-ionospheric electron density and temperature and their variations during geomagnetic activity, Chinese J. Geophys., 54, 2437–2444, 2011 (in Chinese).

Li, M. and Parrot, M.: “Real time analysis” of the ion density measured by the satellite DEMETER in relation with the seismic activity, Nat. Hazards Earth Syst. Sci., 12, 2957–2963, doi:10.5194/nhess-12-2957-2012, 2012.

Lin, C. H., Wang, W., Hagan, M. E., Hsiao, C. C., Immel, T. J., Hsu, M. L., Liu, J. Y., Paxton, L. J., Fang, T. W., and Liu, C. H.: Plausible effect of atmospheric tides on the equatorial ionosphere observed by the FORMOSAT-3/COSMIC: Three-dimensional electron density structures, Geophys. Res. Lett., 34, L11112, doi:10.1029/2007GL029265, 2007a.

Lin, C. H., Hsiao, C. C., Liu J. Y., and Liu, C. H.: Longitudinal structure of the equatorial ionosphere: Time evolution of the four-peaked EIA structure, J. Geophys. Res., 112, A12305, doi:10.1029/2007JA012455, 2007b.

Liu, J., Wan, W., Huang, J., Zhang, X., Zhao, S., Ouyang, X., and Zeren, Z.: Electron density perturbation before Chile M8.8 earthquake, Chinese J. Geophys., 54, 2717–2725, 2011 (in Chinese).

Liu, L., Zhao, B., Wan, W., Venkartraman, S., Zhang, M. L., and Yue, X.: Yearly variations of global plasma densities in the topside ionosphere at middle and low latitudes, J. Geophys. Res., 112, A07303, doi:10.1029/2007JA012283, 2007.

Molchanov, O. A., Hayakaya, M., and Rafalsky, V. A.: Penetration characteristics of electromagnetic emissions from an underground seismic source into the atmosphere, ionosphere,and magnetosphere, J. Geophys. Res., 100, 1691–1712, 1995.

Nemec, F., Santolík, O., and Parrot, M.: Decrease of intensity of ELF/VLF waves observed in the upper ionosphere close to earthquakes: A statistical study, J. Geophys. Res., 114, A04303, doi:10.1029/2008JA013972, 2009.

Oyama, K. I., Watanabe, S., Su, Y., Takanashi, T., and Hirao, K.: Season, local time, and longitude variations of electron temperature at the height of ∼600 km in the low latitude region, Adv. Space Res., 18, 269–278, 1996.

Oyama, K. I., Kakinami, Y., Liu, J. Y., Kamogawa, M., andKodama, T.: Reduction of electron temperature in low-latitude ionosphere at 600 km before and after large earthquakes, J. Geophys. Res., 113, A11317, doi:10.1029/2008JA013367, 2008.

Parrot, M., Berthelier, J. J., Lebreton, J. P., Sauvaud, J. A., Santolik, O., and Blecki, J.: Examples of unusual ionospheric observations made by the DEMETER satellite over seismic regions, Phys. Chem. Earth, 31, 486–495, 2006.

Parrot, M.: Statistical analysis of automatically detected ion density variations recorded by DEMETER and their relation to seismic activity, Ann. Geophys., 55, 149–155, 2012, http://www.ann-geophys.net/55/149/2012/.

Pisa, D., Parrot, M., and Santolík, O.: Ionospheric density variations recorded before the 2010 Mw 8.8 earthquake in Chile, J. Geophys. Res., 116, A08309, doi:10.1029/2011JA016611, 2011.

Pisa, D., Nemec, F., Parrot, M., and Santolik, O.: Attenuation of electromagnetic waves at the frequency ∼1.7 kHz in the upper ionosphere observed by the DEMETER satellite in the vicinity of earthquakes, Ann. Geophys., 55, 157–163, 2012, http://www.ann-geophys.net/55/157/2012/.

Pulinets, S. A.: Ionospheric precursors of earthquakes;recent advances in theory and practical applications, Atmos. Ocean. Sci., 15, 413–415, 2004.

Pulinets, S. A.: Physical mechanism of the vertical electric field generation over active tectonic faults, Adv. Space Res., 44, 767–773, 2009.

Ren, Z., Wan, W., Liu, L., Zhao, B., Wei, Y., Yue, X., and Heelis, R. A.: Longitudinal variations of electron temperature and total ion density in the sunset equatorial topside ionosphere, Geophys. Res. Lett., 35, L05018, doi:10.1029/2007GL032998, 2008.

Rich, F. J., Sultan, P. J., and Burke, W. J.: The 27-day variations of plasma densities and temperatures in the topside ionosphere, J. Geophys. Res., 108, 1297, doi:10.1029/2002JA009731, 2003.

Sarkar, S., Gwal, A. K., and Parrot, M.: Ionospheric variations observed by the DEMETER satellite in the mid-latitude region during strong earthquakes, J. Atmos. Sol.-Terr. Phys., 69, 1524–1540, 2007.

Sarkar, S., Choudhary, S., Sonakia, A., Vishwakarma, A., and Gwal, A. K.: Ionospheric anomalies associated with the Haiti earthquake of 12 January 2010 observed by DEMETER satellite, Nat. Hazards Earth Syst. Sci., 12, 671–678, doi:10.5194/nhess-12-671-2012, 2012.

Shama, D. K., Bardhan, A., and Rai, J.: Ionospheric electron and ion temperatures response to seismic activity, Ind. J. Radio Space Phys., 42, 18–26, 2013.

Sorokin, V. M., Yaschenko, A. K., and Hayakawa, M.: A perturbation of DC electric field caused by light ion adhesion to aerosols during the growth in seismic-related atmospheric radioactivity, Nat. Hazards Earth Syst. Sci., 7, 155–163, doi:10.5194/nhess-7-155-2007, 2007.

Su, Y. Z., Oyama, K. I., Bailey, G. J., Fukao, S., Takahashi, T., and Oya, H.: Longitudinal variations of the topside ionosphere at low latitudes: Satellite measurements and mathematical modelings, J. Geophys. Res., 101, 17191–17205, 1996.

Venkatraman, S. and Heelis, R.: Longitudinal and seasonal variations in nighttime plasma temperatures in the equatorial topside ionosphere during solar maximum, J. Geophys. Res., 104, 2603–2611, 1999.

Zeng, Z., Zhang, B., Fang, G., Wang, D., and Yin, H.: The analysis of ionospheric variations before Wenchuan earthquake with DEMETER data, Chinese J. Geophys., 52, 13–22, 2009 (in Chinese).

Zhang, S. R., Holt, J. M., Zalucha, A. M., and Amory-Mazaudier, C.: Midlatitude ionospheric plasma temperature climatology and empirical model based on Saint Santin incoherent scatter radar data from 1966 to 1987, J. Geophys. Res., 109, A11311, doi:10.1029/2004JA010709, 2004.

Zhang, X., Shen, X., Liu, J., Ouyang, X., Qian, J., and Zhao, S.: Analysis of ionospheric plasma perturbations before Wenchuan earthquake, Nat. Hazards Earth Syst. Sci., 9, 1259–1266, doi:10.5194/nhess-9-1259-2009, 2009.

Zhang, X., Shen, X., Liu, J., Ouyang, X., Qian, J., and Zhao, S.: Ionospheric perturbations of electron density before the Wenchuan Earthquake, Int. J. Remote Sens., 31, 3559–3569, 2010a.

Zhang, X., Liu, J., Shen, X., Parrot, M., Qian, J., Ouyang, X., Zhao, S., and Huang, J.: Ionospheric perturbations associated with the M8.6 Sumatra earthquake on 28 March 2005. Chinese J. Geophys., 53, 567–575, 2010b (in Chinese).

Zhang, X., Zeren, Z., Parrot, M„ Battiston, R., Qian, J., and Shen, X.: ULF/ELF ionospheric electric field and plasma perturbations related to Chile earthquakes, Adv. Space Res., 47, 991–1000, 2011.

Zhang, X., Chen, H., Liu, J., Shen, X., Miao, Y., Du, X., and Qian, J.: Ground-based and satellite DC-ULF electric field anomalies around Wenchuan M8.0 earthquake, Adv. Space Res., 50, 85–95, 2012a.

Zhang, X., Shen, X., Parrot, M., Zeren, Z., Ouyang, X., Liu, J., Qian, J., Zhao, S., and Miao, Y.: Phenomena of electrostatic perturbations before strong earthquakes (2005–2010) observed on DEMETER, Nat. Hazards Earth Syst. Sci., 12, 75–83, doi:10.5194/nhess-12-75-2012, 2012b.

Zhang, X., Shen, X., Zhao, S., Yao, L., Ouyang, X., and Qian, J.: The characteristics of quasistatic electric field perturbations observed by DEMETER satellite before large earthquakes, J. Asian Earth Sci., 79, 42–52, 2014.